High-precision relativistic atomic structure calculations and the EBIT: Tests of QED in highly-charged ions

K. T. Cheng, M. H. Chen, W. R. Johnson, and J. Sapirstein

Abstract: High-precision relativistic atomic structure calculations based on the relativistic many-body perturbation theory and the relativistic configuration-interaction method are shown to provide stringent tests of strong-field quantum electrodynamic (QED) corrections when compared with electron beam ion trap measurements of the spectra of highly-charged, many-electron ions. It is further shown that theory and experiment are accurate enough to test not just the leading screened QED corrections but also smaller contributions from higher-order Breit interactions, relaxed-core QED corrections, two-loop Lamb shifts, negative-energy state corrections, nuclear polarizations and nuclear recoils.

PACS Nos.: 31.30.Jv, 32.30.Rj, 31.25.-v, 31.15.Ar

1. Introduction

Relativistic atomic structure calculations are important for tests of quantum electrodynamic (QED) corrections in high-Z, many-electron ions where binding effects from the strong nuclear fields must be treated nonperturbatively to all orders in the $Z\alpha$-expansion and where screening corrections to electron self-energies and vacuum polarizations are significant. Early tests of QED in high-Z ions were based mostly on the multiconfiguration Dirac-Fock (MCDF) method [1]. An example was given in the work of Seely *et al.* in the mid-80's where laser-plasma measurements of the $4s - 4p$ transition energies in Cu-like ions with $Z = 79 - 92$ were compared with MCDF results [2]. While QED corrections were found to improve the agreement between theory and experiment, residual discrepancies remained very large and were attributed to uncertainties in QED corrections which were basically order-of-magnitude estimates obtained from the $n = 2$ hydrogenic self-energy results of Mohr [3] by $1/n^3$ scalings and by *ad hoc* screening corrections. However, Cheng and Wagner [4] soon pointed out that discrepancies between theory and experiment were actually due to the neglect of finite nuclear size corrections to the atomic transition energies by Seely *et al.* As shown in Fig. 1, theory and experiment actually agree very well when finite nuclear size and QED corrections are both included.

In spite of this apparent success, MCDF calculations are generally not accurate enough for reliable tests of QED corrections. This is clearly demonstrated by the electron beam ion trap (EBIT) measurements of the $2s-2p_{3/2}$ transition energies in three- to ten-electron uranium ions [5]. As shown in Fig. 2,

K. T. Cheng[1] and M. H. Chen. University of California, Lawrence Livermore National Laboratory, Livermore, CA 94550, USA
W. R. Johnson and J. Sapirstein. Department of Physics, University of Notre Dame, Notre Dame, IN 46556, USA

[1]Corresponding author (e-mail: ktcheng@llnl.gov).

 DOI: 10.1139/Z*xx-xxx* © 2007 NRC Canada

Fig. 1. Differences between theory and experiment on the $4s - 4p_{3/2}$ transition energies (eV) of Cu-like ions. Dashed lines show MCDF results of Seely *et al.* [2] without finite nuclear size corrections. Solid lines show MCDF results of Cheng and Wagner [4] with finite nuclear size corrections. Open and solid circles show MCDF results without and with QED corrections, respectively.

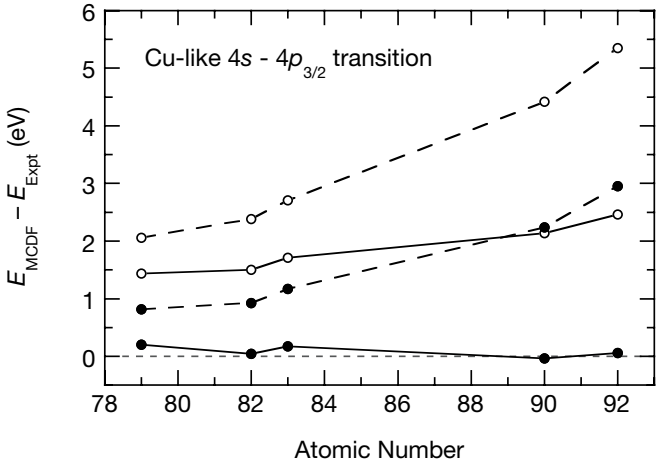

discrepancies between MCDF theory and experiment steadily increase from less than 2 eV in Li-like uranium to 8 eV in Ne-like uranium. These discrepancies are due mainly to inadequate treatments of electron correlations in MCDF calculations as confirmed by relativistic many-body perturbation theory (RMBPT) [6] and relativistic configuration-interaction (RCI) [7] calculations. As shown in Fig. 2, RMBPT and RCI energies, which included directly calculated QED corrections, are in much better agreements with experiment. While RMBPT energies for Be- and Ne-like uranium do deviate from the measured values due to the uncalculated third- and higher-order perturbation corrections which are important for these ions, RCI calculations are intrinsically all-order calculations and RCI energies are seen to agree with the measured energies consistently to within experimental uncertainties. With experimental and RCI uncertainties both at the level of a few tenths of an eV, QED corrections, at about 39 eV in all these $2s - 2p_{3/2}$ transitions, were readily tested to the 1% level.

Advances in theory and experiment have since made possible more stringent tests of QED. In the following, we shall first give a brief descriptions of relativistic atomic structure calculations based on the RMBPT and RCI methods as well as strong-field, correlated QED calculations. We shall then show tests of QED in high-Z ions when RMBPT and RCI results are compared with high-precision EBIT measurements. In particular, the importance of relaxed-core QED and two-loop Lamb shifts will be discussed, along with non-radiative corrections from higher-order Breit interactions, negative-energy state correlations, nuclear polarizations and nuclear recoils.

2. Theory

Relativistic atomic structure and QED calculations pose subtle conceptual difficulties as well as formidable technical challenges. Brief descriptions of the key features of these calculations will be given in this section. More detailed theoretical and computational discussions can be found in the quoted references. A review of the RMBPT and RCI calculations is also given in Ref. [8].

©2007 NRC Canada

Fig. 2. Differences between theory and experiment on the $2s - 2p_{3/2}$ transition energies (eV) of uranium ions. The solid line shows MCDF results. Inverted triangles are RMBPT results. Circles are RCI results. Dotted lines indicate experimental uncertainties. Spectral line identifications are given in Ref. [5].

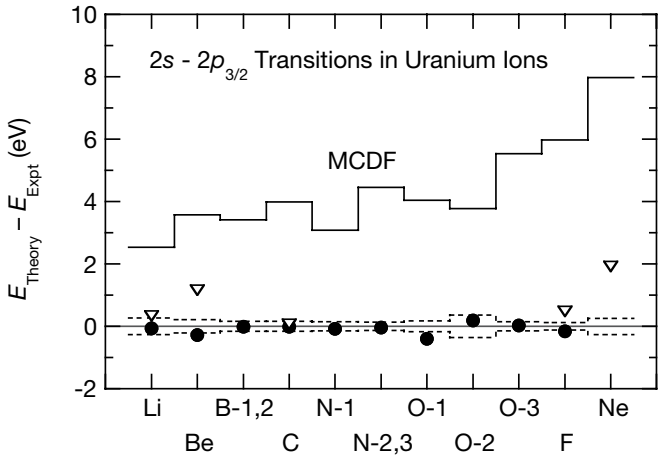

2.1. The no-pair Hamiltonian

Relativistic atomic structure calculations usually start from the many-electron Dirac Hamiltonian which is given in the Coulomb gauge by

$$H_{\rm Dirac} = \sum_{i=1}^{N} h_i + \big(H_{\rm C} + H_{\rm B}\big), \tag{1}$$

where

$$h_i = c\,\vec{\alpha}_i \cdot \vec{p}_i + (\beta_i - 1)mc^2 + V_{\rm nuc}(r_i) \tag{2}$$

is the one-electron Dirac Hamiltonian with the rest mass of the electron subtracted out,

$$H_{\rm C} = \sum_{i>j} \frac{e^2}{r_{ij}} \tag{3}$$

is the Coulomb interaction between the electrons, and

$$H_{\rm B} = -\sum_{i>j} \frac{e^2}{r_{ij}} \left[\vec{\alpha}_i \cdot \vec{\alpha}_j \cos k_0 r_{ij} - (\vec{\alpha}_i \cdot \vec{\nabla}_i)(\vec{\alpha}_j \cdot \vec{\nabla}_j) \frac{\cos k_0 r_{ij} - 1}{k_0^2}\right] \tag{4}$$

is the frequency-dependent Breit interaction with $k_0 = \omega/c$. The nuclear potential is given by $V_{\rm nuc}(r) = -Ze^2/r$ for point-Coulomb potentials, but it can be modified to include nuclear charge distributions to account for finite nuclear size corrections.

While the many-electron Dirac Hamiltonian is widely used in relativistic atomic structure calculations including the MCDF, it is nevertheless known to be problematic. Specifically in relativistic calculations, the existence of negative-energy states, which enter into sums over intermediate states in perturbation theory, results in the "continuum dissolution" problem, also known as the Brown-Ravenhall disease [9], in many-electron systems. Using the $1s^2$ ground state of helium-like ions as

©2007 NRC Canada

an example, this problem can be readily demonstrated with the second-order Coulomb energy

$$E^{(2)} = -\frac{1}{2}\sum_{abmn}\frac{v_{abmn}\tilde{v}_{mnab}}{\epsilon_m+\epsilon_n-\epsilon_a-\epsilon_b}\,, \tag{5}$$

where $v_{ijkl} = \langle ij|H_{\rm C}|kl\rangle$ is the two-electron Coulomb matrix element, $\tilde{v}_{ijkl} = v_{ijkl} - v_{ijlk}$, and ϵ_i is the eigenenergy of the basis state $|i\rangle$ satisfying the one-electron Dirac equation $h|i\rangle = \epsilon_i|i\rangle$. If an intermediate state $|m_+n_-\rangle$ consists of one $1s$ electron, denoted by a, being promoted to a positive-energy continuum state $|m_+\rangle$ with an energy $\epsilon_{m_+} = \epsilon_a + \Delta\epsilon > 0$, while the other $1s$ electron, denoted by b, being demoted to a negative-energy continuum state $|n_-\rangle$ with an energy $\epsilon_{n_-} = \epsilon_b - \Delta\epsilon < -2mc^2$, the denominator, $\epsilon_{m_+} + \epsilon_{n_-} - \epsilon_a - \epsilon_b$, in the above equation would vanish. In effect, any bound state in a many-electron system is degenerate in energy with an infinite number of electron-positron continuum states, as long as $\epsilon_{m_+} + \epsilon_{n_-} = \epsilon_a + \epsilon_b$.

However, the fact that the denominator of $E^{(2)}$ can go to zero is not necessarily a problem. The same situation is encountered in the autoionization of atoms. Since an autoionizing state is embedded in the positive-energy continuum, second- and higher-order perturbations will also lead to vanishing energy denominators. In that case, an infinitesimal imaginary part must be added to the denominator, with the result that the principal part of the matrix element leads to a real energy shift while the imaginary part to an autoionization line width. But this is where the analogy ends. An autoionizing line width from the imaginary part of the energy denominator here would mean that there are no stable ground states for many-electron systems, as they can decay by "autoionizing" into the electron-positron continuum. The stability of atomic ground states is, of course, explained by the fact that the negative-energy sea is filled and that spontaneous pair production is prohibited by the Pauli exclusion principle. Here lies the real problem with the many-electron Dirac Hamiltonian: it has no provision to account for this fact and hence cannot prevent the decay of positive-energy electrons into the negative-energy continuum. The standard cure is to use the no-pair Hamiltonian

$$H_{\rm no-pair} = \sum_{i=1}^{N} h_i + \Lambda_{++}\big(H_{\rm C} + H_{\rm B}\big)\Lambda_{++} \tag{6}$$

which excludes negative-energy states entirely by the use of the positive-energy projector Λ_{++} [10, 11]. This is the starting point of our RCI and RMBPT calculations and should be the starting point of any high-precision relativistic atomic structure calculations.

Nevertheless, the use of the no-pair Hamiltonian does entail some compromises. Specifically in nonrelativistic CI calculations, eigenenergies saturated with large configuration expansions are independent of the basis functions used. Such is not the case here. By starting from the no-pair Hamiltonian and neglecting negative-energy states, relativistic basis sets are truncated and RCI as well as RMBPT results are, in general, gauge and basis set dependent. Numerically, this has been demonstrated by Sapirstein *et al.* [12] who showed that the ground state RCI energy of helium-like uranium as calculated with the no-pair Hamiltonian depends on the potential used in generating the one-electron basis functions. These authors further showed that this potential dependence can be eliminated mathematically by completing the basis set to include both the positive- and negative-energy orbitals. However, while the inclusion of negative-energy basis functions, which is equivalent to using the full Dirac Hamiltonian, does lead to potential independent results, it was found that the $1s^2$ ground state is no longer the lowest eigenstate of the RCI matrix and is now surrounded by spurious energy levels characterized by configurations with one positive- and one negative-energy electrons. In effect, that was a numerical demonstration of the Brown-Ravenhall disease where the $1s^2$ ground state is embedded in a discrete representation of the (unphysical) electron-positron continuum when negative-energy basis functions are also used in RCI calculations. These results can be found in Table III of Ref. [12], along with more detailed discussions in that reference.

©2007 NRC Canada

Fig. 3. Ladder and crossed ladder diagrams for second-order correlation energies.

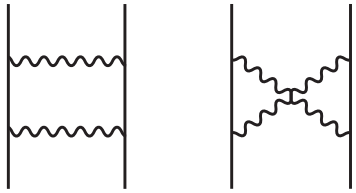

While there are no numerical disasters from vanishing denominators in RCI calculations when negative-energy basis functions are used, results of the full Dirac Hamiltonian, though potential independent, are nevertheless incorrect. To see this, we note that if the sum over intermediate states for the second-order energy is extended to included both positive- and negative-energy states, $E^{(2)}$ in Eq. (5) can be rewritten as

$$\begin{aligned} E^{(2)}_{\rm Dirac} &= -\frac{1}{2}\sum_{abm_+n_+}\frac{v_{abm_+n_+}\tilde{v}_{m_+n_+ab}}{\epsilon_{m_+}+\epsilon_{n_+}-\epsilon_a-\epsilon_b}-\frac{1}{2}\sum_{abm_-n_-}\frac{v_{abm_-n_-}\tilde{v}_{m_-n_-ab}}{\epsilon_{m_-}+\epsilon_{n_-}-\epsilon_a-\epsilon_b} \\ &\quad -\frac{1}{2}\sum_{abm_+n_-}\frac{v_{abm_+n_-}\tilde{v}_{m_+n_-ab}}{\epsilon_{m_+}+\epsilon_{n_-}-\epsilon_a-\epsilon_b}-\frac{1}{2}\sum_{abm_-n_+}\frac{v_{abm_-n_+}\tilde{v}_{m_-n_+ab}}{\epsilon_{m_-}+\epsilon_{n_+}-\epsilon_a-\epsilon_b}\,. \end{aligned} \tag{7}$$

The first and second terms in the right-hand-side of Eq. (7) come from virtual electron-electron and positron-positron pairs in the intermediate states, respectively, while the third and fourth terms are from electron-positron pairs. $E^{(2)}_{\rm Dirac}$ can be compared with rigorous second-order correlation energy $E^{(2)}_{\rm QED}$ which have been calculated in the S-matrix formalism of QED from the ladder (L) and crossed ladder (X) diagrams shown in Fig. 3. When these diagrams are taken together, $E^{(2)}_{\rm QED}=E_L+E_X$ have been shown to be gauge invariant [13, 14]. Formulas for E_L and E_X with the exchange of two Coulomb photons are given by [12]

$$E_L = -\frac{1}{2}\sum_{abm_+n_+}\frac{v_{abm_+n_+}\tilde{v}_{m_+n_+ab}}{\epsilon_{m_+}+\epsilon_{n_+}-\epsilon_a-\epsilon_b}+\frac{1}{2}\sum_{abm_-n_-}\frac{v_{abm_-n_-}\tilde{v}_{m_-n_-ab}}{\epsilon_{m_-}+\epsilon_{n_-}-\epsilon_a-\epsilon_b}\,, \tag{8}$$

$$\begin{aligned} E_X &= -\frac{1}{2}\sum_{abm_+n_-}\frac{v_{an_-m_+b}\,v_{bm_+n_-a}-v_{an_-m_+a}\,v_{bm_+n_-b}}{\epsilon_{n_-}-\epsilon_{m_+}} \\ &\quad -\frac{1}{2}\sum_{abm_-n_+}\frac{v_{an_+m_-b}\,v_{bm_-n_+a}-v_{an_+m_-a}\,v_{bm_-n_+b}}{\epsilon_{m_-}-\epsilon_{n_+}}\,. \end{aligned} \tag{9}$$

It can be seen that the ladder diagram has the same electron-electron term as $E^{(2)}_{\rm Dirac}$, but its positron-positron term has an opposite sign. More importantly, electron-positron terms, which come from the crossed ladder diagram only, are very different from those in $E^{(2)}_{\rm Dirac}$ and their denominators, which are given by $\epsilon_{m_+}-\epsilon_{n_-}$, will not vanish. Thus, the correct field-theoretic treatment of relativistic correlation energies is shown to be free of the Brown-Ravenhall disease, as it should be.

When negative-energy states are excluded, both $E^{(2)}_{\rm Dirac}$ and $E^{(2)}_{\rm QED}$ reduce to the same no-pair energy

$$E^{(2)}_{\rm no-pair}=-\frac{1}{2}\sum_{abm_+n_+}\frac{v_{abm_+n_+}\tilde{v}_{m_+n_+ab}}{\epsilon_{m_+}+\epsilon_{n_+}-\epsilon_a-\epsilon_b}\,, \tag{10}$$

©2007 NRC Canada

which is usually a good enough approximation to the true correlation energy $E^{(2)}_{\rm QED}$. High-precision relativistic atomic structure calculations can thus be carried out with the no-pair Hamiltonian to sufficiently high orders of perturbations for accurate correlation results. Residual contributions from the negative-energy states are usually quite negligible except for very high-Z ions and can be adequately obtained from the second-order energies $E^{(2)}_{\rm QED} - E^{(2)}_{\rm no-pair}$. An example of these corrections will be given later. It should be noted that errors in $E_{\rm Dirac}$ from incorrect treatments of electron-positron and positron-positron terms can be very subtle. Nevertheless, it is very difficult, if not impossible, to identify and correct the intrinsic errors in $E_{\rm Dirac}$ and the use of the many-electron Dirac Hamiltonian should be avoided even if it appears to be giving sensible results.

2.2. B-Spline basis functions

The proper choice of finite basis functions is important to RMBPT and is critical to RCI calculations. For RMBPT, the main issue is the completeness of the basis set for carrying out sums over intermediate states in second- and higher order perturbations. For RCI, the problem is more complicated. In nonrelativistic atomic and molecular CI calculations, a wide range of finite basis sets such as the Slater-type and Gaussian-type orbitals have been used successfully. Relativistically, the construction of positive-energy projection operators can be a daunting task and the no-pair requirement is often ignored in RCI calculations. More problematically, since the energy functional is not bounded from below due to the existence of the negative-energy states in relativistic calculations, expansions of the 4-component spinor wave functions in terms of finite basis sets is known to lead to variational instabilities in RCI calculations and to drastic problems such as the appearance of spurious eigenstates and the "variational collapse" of eigenenergies. These problems are not limited to many-electron systems and can affect hydrogenic ions also. In most cases, variational constraints such as the "kinetic balance" condition [15, 16] are imposed to bring these problems under control. Even so, additional constraints may still be needed to maintain variational stabilities [16].

However, even if there is no instability problem associated with the basis functions, there is still the question of whether the correct nonrelativistic limit can be reached when the fine structure constant α approaches zero. As an example, MCDF calculations, which are RCI calculations using MCDF basis functions obtained by solving a set of coupled differential equations self-consistently, are free of the variational collapse problem. The trouble is that the inhomogeneous configuration-mixing terms in the MCDF equations do not necessarily have correct nonrelativistic limits and can lead to erroneous fine structure results. In some cases, *ad hoc* corrections have to be made by explicitly subtracting out the spurious contributions that remain in the nonrelativistic limit. (See, for example, Ref. [17].) MCDF is a powerful method but is probably not suitable for high-precision calculations.

For our RMBPT and RCI calculations, we use the B-spline finite basis set method developed by Johnson *et al.* [18]. B-spline orbitals are Dirac orbitals of an electron moving in a model potential confined to a finite cavity. They are expanded in terms of B-spline, or basis-spline, functions which are piecewise polynomials in an interval divided into segments, and expansion coefficients are obtained by solving a generalized eigenvalue problem set up by the one-electron Dirac equation subjected to the boundary condition imposed by the MIT bag model [19] at the cavity boundary to ensure that electrons are confined without evoking the difficulty associated with the Klein paradox [20].

B-spline orbitals form finite, complete basis sets as confirmed by sum rule calculations [18] and are ideally suited for RMBPT calculations involving sums over intermediate states. They also cleanly separated into positive- and negative-energy states so that the no-pair requirement can easily be implemented by using only positive-energy B-spline orbitals which readily provide an accurate, discrete representation of the bound and continuum states for high-precision correlation calculations. There are additional benefits for using them in RCI calculations. As solutions of the homogeneous one-electron Dirac equation, B-spline orbitals reduce to the correct nonrelativistic limit when $\alpha \to 0$ and there are no spurious states in the one-electron spectra. Along with the completeness of these finite basis func-

©2007 NRC Canada

Fig. 4. One-loop self-energy and vacuum polarization diagrams.

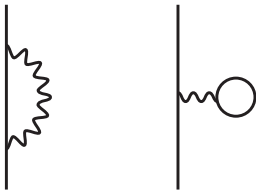

tions, the kinetic balance condition is implicitly satisfied and there are no known variational instability problems. The down side is that these are not highly optimized basis functions and can lead to very large-scale RCI calculations. But with advances in high-performance computers, that is no longer an insurmountable problem. Recent RCI calculations using B-spline basis functions have reached close to half a million configurations. Davidson's method [21] as implemented by Stathopoulos and Froese Fischer [22] is used to solve these large RCI matrices for the first few eigenstates. Correlation contributions from single-, double-, triple-, ... excitations can be systematically included in the form of valence-valence, core-valence and core-core excitations for very well converged RCI results.

In our RMBPT and RCI calculations, nuclear charge distributions are included in the nuclear potential $V_{\rm nuc}(r)$ for generating one-electron B-spline basis orbitals to account for the finite nuclear size effect. Parameters for the Fermi charge distributions are obtained from Johnson and Soff [23], except for thorium and uranium where they are obtained from the measurements by Zumbro *et al.* [24, 25].

2.3. QED calculations

Screened QED corrections shown in the following section are calculated directly from the one-loop self-energy and vacuum polarization diagrams shown in Fig. 4. Self-energies are calculated nonperturbatively to all orders of $Z\alpha$ in the external potential with partial wave expansions in the configuration space using numerical bound-state Green's functions. Subtraction terms involving the free-electron propagator are evaluated in momentum space, which requires accurate Fourier-transformed wave functions. Details of these self-energy calculations, with references to earlier works, can be found in Ref. [26]. As for vacuum polarizations, leading contributions are obtained from expectation values of the Uehling potential, while higher-order Wichmann-Kroll corrections, like the self-energies, are calculated nonperturbatively in the external potential with partial wave expansions in the configuration space using numerical bound-state Green's functions [27]. Total QED corrections to many-electron ions are then given by the sum of one-electron QED contributions, weighted by the generalized occupation numbers of the valence electrons.

For many-electron ions, correlation corrections to the one-loop radiative diagrams are significant. Examples of these radiative correlation diagrams are shown in Fig. 5. As pointed out by Blundell [28], screening corrections to the valence electron of an alkali-like ion from direct-interaction diagrams such as those shown in Figs. 5(a) – 5(d) can be accounted for exactly by evaluating the one-loop diagrams with a "core-Hartree" potential $V(r)$ such that

$$V(r) = V_{\rm nuc}(r) + e^2 \int_0^r dr' \frac{1}{r_>} \rho(r'), \tag{11}$$

where $\rho(r)$ is the radial charge density of the closed core

$$\rho(r) = \sum_c (2j_c + 1)\rho_c(r). \tag{12}$$

©2007 NRC Canada

Fig. 5. Typical QED correlation diagrams.

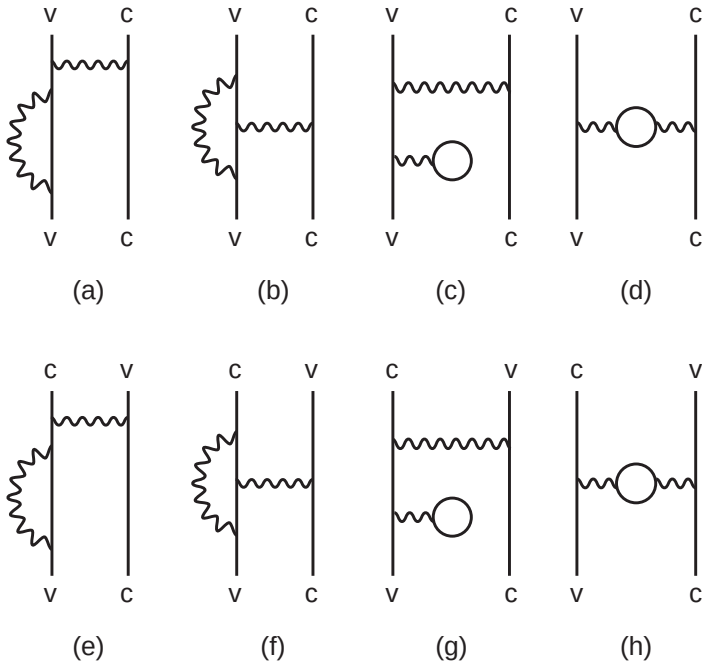

In particular, $\rho_c(r) = g_c^2(r) + f_c^2(r)$ is the radial charge density of a core electron c and $g_c(r)$ and $f_c(r)$ are the upper and lower components of the radial Dirac wave functions determined self-consistently by the Dirac-Hartree equation of the closed core. Likewise, a core electron can be screened by other core electrons as well as by the valence electron in a "modified core-Hartree" potential with the charge density

$$\rho(r) = \rho_v(r) + \sum_c{}' (2j_c + 1)\rho_c(r), \tag{13}$$

where v and c refer to valence and core electrons, respectively, and the sum $\sum'$ goes over one less core electron from the same subshell. Core screening diagrams are the same as those shown in Figs. 5(a) – 5(d), but with the core- and valence-electron indices "c" and "v" interchanged. Blundell further calculated exchange-interaction "side" diagrams such as those shown in Figs. 5(e) and 5(g) as one-loop diagrams with perturbed orbitals, but exchange-interaction "vertex" diagrams such as those shown in Figs. 5(f) and 5(h) were ignored with the expectation that their contributions should be small.

In our QED calculations, one-loop radiative diagrams are evaluated with N-electron Dirac-Kohn-Sham (DKS) potentials instead of $(N-1)$-electron core-Hartree or modified core-Hartree potentials. This is equivalent to using the total charge density of the atomic state

$$\rho(r) = \rho_v(r) + \sum_c (2j_c + 1)\rho_c(r) \tag{14}$$

and adding to $V(r)$ an average exchange potential

$$V_{\rm ex} = -x_\alpha \frac{e^2}{r} \left[\frac{81}{32\pi^2}\, r\, \rho(r)\right]^{1/3}. \tag{15}$$

©2007 NRC Canada

In particular, $x_\alpha = 0$, 2/3 and 1 for Hartree, Kohn-Sham and Slater averaged-exchange potentials, respectively. With N-electron DKS potentials, self-interaction contributions will not cancel exactly between the direct- and exchange-interaction diagrams, but these residual corrections should be quite small. Computationally, they have the advantage over core-Hartree and modified core-Hartree potentials in that the same screening potential is used for QED calculations of all electrons in an atomic state. Once one-electron QED energies ϵ_i are calculated for each subshell i, total QED correction to the energy level of an alkali-like ions is given by

$$E_{\rm QED} = \epsilon_v + \sum_c (2j_c + 1)\epsilon_c. \tag{16}$$

For many-electron ions, ϵ_v in the above equation can be replaced by $\sum_v q_v \epsilon_v$, where q_v are the generalized occupation numbers of the valence electrons.

Our early QED calculations are carried out in a "frozen-core" approximation where the same potential is used to calculate the ϵ's for both the initial and final states. As a result, there is no contributions from the core electrons, and QED corrections to transition energies are simply given by differences in ϵ_v's for alkali-like ions and by differences in the configuration-weighted sums of ϵ_v's for multi-valence electron ions. However, contributions from the core electrons, though small, are not completely negligible. To account for "relaxed-core" effects, we use DKS potentials specific to the initial- and final-state valence configurations. This leads to slightly different one-electron QED energies for the same core and valence electrons in the initial and final states, and core-electron contributions no longer cancel exactly. As we shall show in the following, these relaxed-core corrections are indeed very important.

It should be noted that QED corrections thus calculated will be potential dependent. The key is to choose model potentials that minimize contributions from uncalculated higher-order QED correlation diagrams. DKS potentials are used because they have been found to give very accurate QED energies for the $2s - 2p$ transitions in high-Z Li- and Be-like ions [29], the $3s - 3p$ transitions in Na-like to Si-like uranium ions [30], and the $4s - 4p$ and $4p - 4d$ transitions in heavy Cu-like ions [31, 32]. Some of these results will be shown in the following section.

3. Results and discussions

Reliable relativistic atomic structure and QED calculations have been carried out for a few highly-charged ions where accurate EBIT measurements are available. Comparisons between theory and experiment have not only provided precision tests of QED but also revealed several small corrections which were often ignored. These corrections will be discussed in the following.

3.1. Higher-order Breit corrections

The spectra of the low-lying $n = 2$ states in Li-like ions have been studied with RMBPT [33, 34] and RCI [35]. Comparisons between theory and experiment on the $2s - 2p_{1/2}$ transition energies is shown Fig. 6. It can be seen that RMBPT and RCI are in very good agreement with each other and with experiment throughout the isoelectronic sequence, while MCDF results [36] are clearly not as accurate due to inadequate treatments of correlation energies. Detail comparisons between theory and experiment, including those for the $2s - 2p_{3/2}$ transition, can be found in Ref. [35].

However, RMBPT and RCI results do differ slightly at high Z. This can be seen in the $2s - 2p_{3/2}$ transition energies in Li-like U^{89+} shown in Table 1. Specifically, while RMBPT and RCI Coulomb energies agree to within 0.02 eV, corresponding Breit energies differ by as much as 0.33 eV. This discrepancy is due mainly to the neglect of higher-order Breit interactions in early RMBPT calculations [34] which include contributions only up to the exchange of one transverse photon. Well converged RCI Breit energies, on the other hand, include high-order contributions implicitly. It is interesting to note that when QED corrections are included, RMBPT total energy actually is in better agreement

©2007 NRC Canada

Fig. 6. Li-like $2s - 2p_{1/2}$ transition energies relative to RCI energies [35] are scaled by Z^2. Solid line: MCDF [36]. Triangles: RMBPT [33, 34]. Crosses: Experiments (references given in [35]).

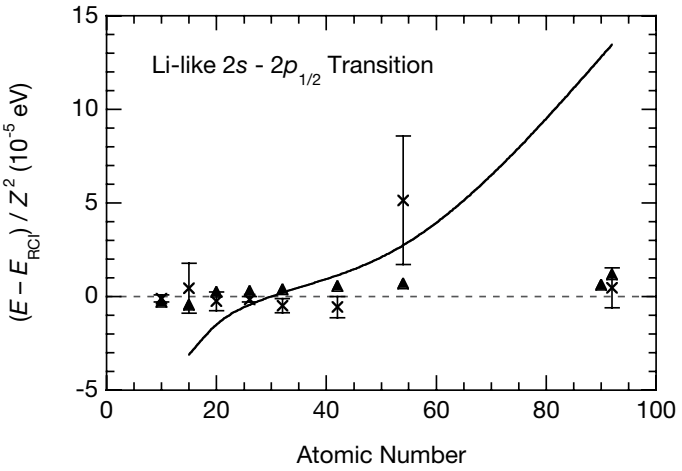

Table 1. The $2s - 2p_{3/2}$ transition energies (eV) of Li-like uranium. RMBPT results are from Ref. [38], RCI results are from [35], and the EBIT data is from [37].

Contribution	RMBPT	RCI
Coulomb	4514.81	4514.79
Breit	-16.22	-15.88
Mass Polarization	-0.04	-0.04
QED	-39.13	-39.69
Theory	4459.43	4459.18
EBIT	4459.37(21)	

with the EBIT measurement [37] than is RCI. But as we shall show in the following, this is largely due to cancellation of errors between the Breit and QED energies. For high-precision atomic structure calculations, contributions from higher-order Breit corrections should be included.

3.2. Relaxed-core QED corrections

For the $2s - 2p_{3/2}$ transition, high-precision EBIT measurements are available for Li-like Bi^{80+}, Th^{87+} and U^{89+}. By subtracting RCI energies from their EBIT data, Beiersdorfer *et al.* have deduced empirical QED corrections which were found to disagree with all existing theories [37]. This is shown in Fig. 7 where empirical QED energies scaled by Z^4 are seen to be in-between the calculated results by Blundell [38] and Chen *et al.* [35]. While uncertainties in Blundell's results are most likely due to the neglect of exchange interactions in the vertex diagram as mentioned earlier, errors in the results of Chen *et al.* were soon found to be due to the use of frozen-core approximation in their QED calculations [29]. As shown in Fig. 7, adding relaxed-core corrections to the frozen-core results leads to relaxed-core QED energies which are in very good agreement with the empirical data. Indeed, for Li-like Bi^{80+}, the relaxed-core correction of +0.17 eV change the frozen-core QED energy of -26.54 eV to the relaxed-core value of -26.37 eV which is in good agreement with the empirical data of -26.33(4) eV. For this particular ion, rigorous QED corrections of the complete set of correlated QED diagrams shown in Fig. 5 have been carried out by Sapirstein and Cheng [39]. Their result of -26.35 eV is in

©2007 NRC Canada

Fig. 7. Scaled QED energies for the $2s - 2p_{3/2}$ transition in Li-like ions. Dotted line: Blundell's results [38]. Dashed line: Frozen-core results of Chen *et al.* [35]. Solid line: Relaxed-core results of Cheng *et al.* [29]. Triangle: Sapirstein and Cheng [39]. Crosses: empirical EBIT data [37].

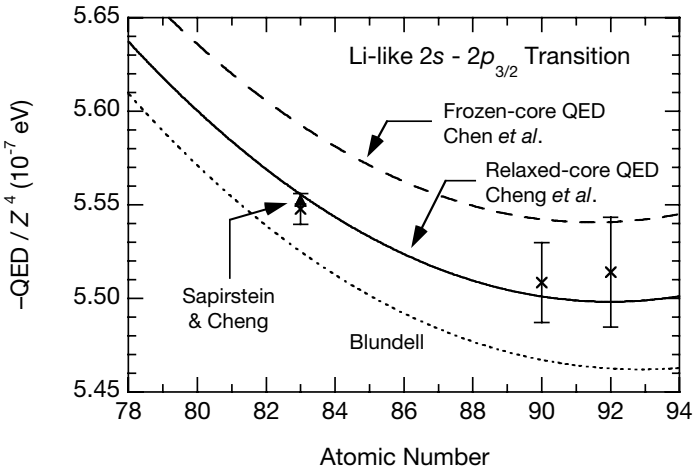

excellent agreement with the relaxed-core and empirical values. From these comparisons, it is clear that relaxed-core QED corrections are important for Li-like ions. As we shall show in the following, this is also true for other high-Z ions with more electrons and more complicated electronic configurations.

3.3. Two-loop Lamb shifts and negative-energy state corrections

Combining the RCI energy of 2814.47 eV with the relaxed-core QED energy of -26.37 eV, Cheng *et al.* [29] obtained a total theoretical energy of 2788.10 eV for the $2s-2p_{3/2}$ transition in Li-like Bi^{80+} which agree with the EBIT value of 2788.139(39) eV [37] to within the experimental uncertainty of 0.04 eV. However, in the work of Sapirstein and Cheng [39] where atomic structure energies and QED corrections for the same transition in Bi^{80+} are carried out in S-matrix calculations consistently up to the exchange of two virtual photons, they found a residual discrepancy of 0.175 eV with the measured data which they attributed to the uncalculated two-loop Lamb shift corrections. This is a relatively large correction and should, but did not, show up in the comparison between the total RCI and the measured EBIT data. Closer inspections show that this is yet another case of cancellation of errors.

Contributions to the $2s - 2p_{3/2}$ transition energy in Li-like Bi^{80+} from the RCI [29] and S-matrix [39] calculations are shown in the second and third columns of Table 2. It can be seen that while the two QED corrections are in good agreement, the two structure energies actually differ by 0.16 eV. Since these structure energies are very well converged, there can only be one possible explanation for this large discrepancy: RCI calculations are based on the no-pair Hamiltonian and, unlike the rigorous S-matrix calculations, do not include correlation contributions from the negative-energy states. Subtracting RCI from the S-matrix structure energy, the difference of -0.16 eV should thus be the negative-energy correction to the RCI energy which, in this case, just happens to largely cancel the +0.175 eV two-loop Lamb shift contribution.

However, two-loop Lamb shifts and negative-energy corrections do not always cancel each other. Such is the case with the $2s - 2p_{1/2}$ transition energy in Li-like U^{89+} that has also been measured to very high precision at the Livermore EBIT by Beiersdorfer *et al.* [40]. RCI, S-matrix and EBIT results are shown in the fourth and fifth columns in Table 2. Subtracting the total S-matrix energy of 280.44 eV from the measured value of 280.645(15) eV, these authors have deduced a two-loop Lamb

©2007 NRC Canada

Table 2. Two-loop Lamb shifts and negative-energy states (NES) contributions. RCI structure and QED energies are from [29]. S-matrix structure and QED energies are from [39]. EBIT data are from [37] and [40] for Bi^{80+} and U^{89+}, respectively.

Contribution	Li-like Bi^{80+} $2s-2p_{3/2}$		Li-like U^{89+} $2s-2p_{1/2}$	
	RCI	S-matrix	RCI	S-matrix
Structure	2814.47	2814.312	322.17	322.21
QED	-26.37	-26.348	-41.72	-41.77
Sum	2788.10	2787.964	280.45	280.44
2-loop	0.175		0.205	
NES	-0.16		0.04	
Theory	2788.115		280.695	
EBIT	2788.139(39)		280.645(15)	

shift of 0.205 eV which is comparable in size to the one for the $2s-2p_{3/2}$ transition in Bi^{80+}. In this case, however, the negative-energy correction to the RCI energy, which is again given by the difference between the RCI and S-matrix structure energies, is much smaller at +0.04 eV and has the same sign as the two-loop Lamb shift. As a result, while the two-loop Lamb shift is obscured by the negative-energy correction in the $2s-2p_{3/2}$ transition in Bi^{80+}, its effect definitely shows up in the $2s-2p_{1/2}$ transition in U^{89+} when RCI energies are compared with experiment. As seen from Table 2, RCI total energies do agree with the measured values to within 0.04 - 0.05 eV in both cases after two-loop Lamb shifts and negative-energy corrections are included.

3.4. Nuclear recoil and nuclear polarization corrections

Besides the finite nuclear size correction, there are two other small nuclear corrections that should be considered in high-precision atomic structure calculations: the polarization and recoil of the nucleus. Nuclear polarization corrections are usually quite negligible except for the nuclei of thorium and uranium ions which are quite polarizable due to the presence of low-lying nuclear excited states. These corrections have been calculated by Plunien and Soff who gave values of 0.14 and 0.20 eV for the $2s-2p$ transitions in Th^{87+} and U^{89+}, respectively [41]. These authors later pointed out that their results were too large by a factor of 2π [42]. At 0.02 - 0.03 eV, the corrected nuclear polarizations were deemed to be too small to matter. However, in view of the recent EBIT measurement of the $2s-2p_{1/2}$ transition energy in Li-like U^{89+} which has reached an accuracy of 0.015 eV, these corrections can no longer be ignored.

The recoil of the nucleus is a very challenging theoretical problem. The leading contribution comes from the mass-polarization term which can easily be evaluated by taking the expectation values of the operator

$$\frac{1}{M}\sum_{i>j}\vec{p}_i\cdot\vec{p}_j, \tag{17}$$

where M is the mass of the nucleus. Leading relativistic corrections come from: i) evaluating the mass-polarization operator with relativistic instead of nonrelativistic wave functions and ii) taking the expectation value of the relativistic operator

$$\frac{1}{M}\sum_{i>j}V_{\rm nuc}(r_i)\Big[\vec{\alpha}_i+\frac{(\vec{\alpha}_i\cdot\vec{r}_i)\vec{r}_i}{r_i^2}\Big]\cdot\vec{p}_j \tag{18}$$

which arises from the exchange of one transverse photon between the nucleus and the atomic electrons. Higher-order corrections from the exchange of two or more transverse photons do not reduce to

©2007 NRC Canada

simple operator forms and must be treated with QED [43] or with the Bethe-Salpeter equation [44]. They have been shown to scale very rapidly with the nuclear charge and are important for high-Z Li-like ions [43]. For the $2s - 2p_{1/2}$ transition in Li-like U^{89+}, starting from Dirac Coulomb wave functions, contributions from the mass polarization term, the one transverse-photon exchange term and the two transverse-photon exchange term have been given by -0.08, +0.06 and -0.05 eV for a total nuclear recoil corrections of -0.07 eV [43]. In previous RMBPT [34] and RCI [29] calculations, the same mass polarization corrections have been evaluated with correlated wave functions and the result of -0.04 eV was included in the RMBPT and RCI structure energies. But this leave a residual nuclear recoil correction of -0.03 eV unaccounted for, which may have canceled the +0.03 eV nuclear polarization correction that has also been left out. Once again, cancellation of errors may complicate the task of identifying these small corrections. But as in the case of two-loop Lamb shifts versus negative-energy corrections, the effect of higher-order nuclear recoils may show up in other high-Z ions where nuclear polarizations, which are quite nucleus dependent, are completely negligible. Further research into nuclear recoils and more high-precision spectral measurements in heavy ions other than thorium and uranium are definitely desirable.

3.5. Na-like to Si-like uranium ions

As further tests of QED corrections in more complicated atomic systems, comparisons have been made between RCI and high-precision EBIT measurements on the energies of several x-ray lines from the $3s - 3p_{3/2}$ transitions in Na-like to Si-like uranium [30]. Results are shown in Table 3. Here, RCI energies include all contributions from single and double excitations in terms of valence-valence, core-valence and core-core excitations, with uncertainties arising mainly from the missing triple and quadruple excitations which are estimated to be about 0.02 eV for the Na-1, Mg-1 and Al-1 lines and about 0.07 eV for the Al-2 and Si-1 lines. Mass polarization corrections, though missing higher-order nuclear recoil contributions, are small at -0.01 eV and are included mainly as order-of-magnitude reminders. As for QED corrections, they are dominated by the self-energies as expected. It is interesting to note that at -0.15 to -0.20 eV, Wichmann-Kroll corrections are about 10 times larger than experimental uncertainties and are very significant. Even relaxed-core corrections to the QED energies, though smaller at 0.08 to 0.14 eV, are important in bringing theory into good agreement with experiment. Uncertainties in QED corrections are estimated to be about 0.07 eV which are due in part to the use of DKS potentials to account for screening corrections and in part to the missing two-loop Lamb shifts and negative-energy corrections which are expected to be much smaller here for the $n = 3$ transitions than in the case of Li-like uranium for the $n = 2$ transitions. Theoretical results as given by the sums of RCI and QED energies are seen to be in excellent agreement with the high-precision EBIT measurements. The only exception is the Si-1 line where the difference between theory and experiment is slightly larger at 0.11 eV. All data shown in Table 3 are from Ref. [30]. More detailed discussions of these results can also be found there.

3.6. Cu-like ions

Until recently, most of the existing tests of QED deal with $ns - np$ transitions and very few, if any, precision tests are available for higher angular momentum states. While QED corrections are expected to be small for high-l bound electrons as the centrifugal barrier $l(l+1)/2r^2$ prevents them from getting too close to the nucleus, their contributions may not be negligible for heavy ions when comparing theory with experiment. Such is the case with the recent EBIT measurements which have produced highly-accurate x-ray energies for the $4s - 4p_{3/2}$ transition in high-Z Cu-like ions [45, 46, 47] and, in particular, for the $4p_{1/2} - 4d_{3/2}$ transition in Cu-like bismuth, thorium and uranium [47]. RMBPT [32, 48] and RCI [31] calculations have also been carried out and were found to give essentially the same results. Comparisons between theory and experiment are shown in Table 4. Once again, they are in very good agreements. For the $4s - 4p_{3/2}$ transition, relaxed-core QED corrections are small and

©2007 NRC Canada

Table 3. Energies (eV) of the $3s - 3p_{3/2}$ transitions in Na-like to Si-like uranium. All results are from [30]. Spectral line identifications can also be found there.

Contributions		Na-1	Mg-1	Al-1	Al-2	Si-1
RCI	Coulomb	1318.14	1329.48	1332.25	1316.00	1319.02
	Breit	-2.79	-2.75	-2.29	-5.99	-5.57
	Mass polarization	-0.01	-0.01	-0.01	-0.01	-0.01
	Sum	1315.34(2)	1326.72(2)	1329.95(2)	1310.00(7)	1313.44(7)
QED	Self-energy	-14.21	-13.99	-13.98	-10.39	-10.59
	Uehling	4.10	4.04	4.03	2.98	3.04
	Wichmann-Kroll	-0.20	-0.20	-0.20	-0.15	-0.15
	Relaxed-core	0.08	0.08	0.08	0.14	0.13
	Sum	-10.23(7)	-10.07(7)	-10.07(7)	-7.42(7)	-7.57(7)
Theory		1305.11(7)	1316.65(7)	1319.88(7)	1302.58(10)	1305.87(10)
EBIT		1305.12(2)	1316.64(1)	1319.86(2)	1302.55(2)	1305.76(2)

Table 4. The $4s - 4p$ and $4p - 4d$ transition energies in high-Z Cu-like ions. RMBPT and QED results are from [32]. EBIT results are from [45, 46, 47].

Z	RMBPT	QED				Total	EBIT
		Frozen	ΔRelaxed	2-Loop	Sum		
				$4s - 4p_{3/2}$			
74	200.13	-1.25	0.01	0.00	-1.24	198.89	198.90(1)
79	255.01	-1.65	0.01	0.01	-1.63	253.38	253.40(1)
82	294.45	-1.93	0.01	0.01	-1.91	292.55	292.59(4)
90	430.03	-2.86	0.02	0.02	-2.82	427.21	427.20(1)
92	472.30	-3.14	0.03	0.02	-3.09	469.21	469.22(3)
				$4p_{1/2} - 4d_{3/2}$			
83	367.21	-0.31	0.05	0.00	-0.27	366.94	366.97(2)
90	492.42	-0.56	0.07	0.00	-0.49	491.93	491.94(10)
92	535.69	-0.66	0.08	0.00	-0.58	535.11	535.15(5)

amount to less than 1% of the total QED energies. For the $4p_{1/2} - 4d_{3/2}$ transition, however, they are surprisingly large and amount to 14% - 18% of the total QED energies. Empirical QED energies for the $4p_{1/2} - 4d_{3/2}$ transition can be deduced from the measured data by subtracting the RMBPT energies. They are compared with QED results calculated with and without the relaxed-core corrections in Fig. 8. For these high-l, high-n states, two-loop Lamb shifts and negative-energy corrections should be quite negligible and relaxed-core corrections, which are up to twice as large as the uncertainties of the empirical data, are seen to be very important in bringing theory into agreement with experiment. QED corrections in high-l states are rarely studied and may contain other surprises that have yet to be discovered.

4. Conclusion

We have shown that relativistic atomic structure calculations from RMBPT and RCI have provided important tests of strong-field QED when compared with high-precision EBIT measurements of the spectra of high-Z ions. In the course of these comparisons, small corrections from higher-order Breit energies, relaxed-core QED, two-loop Lamb shifts, negative-energy states, nuclear polarizations and nuclear recoils have been identified. While the correct treatment of relativistic correlation energies only

©2007 NRC Canada

Fig. 8. Scaled QED energies for the $4p_{1/2} - 4d_{3/2}$ transition in Cu-like ions. Dashed and solid lines are frozen- and relaxed-core calculations [32]. Crosses with error bars are empirical data based on EBIT measurements [47].

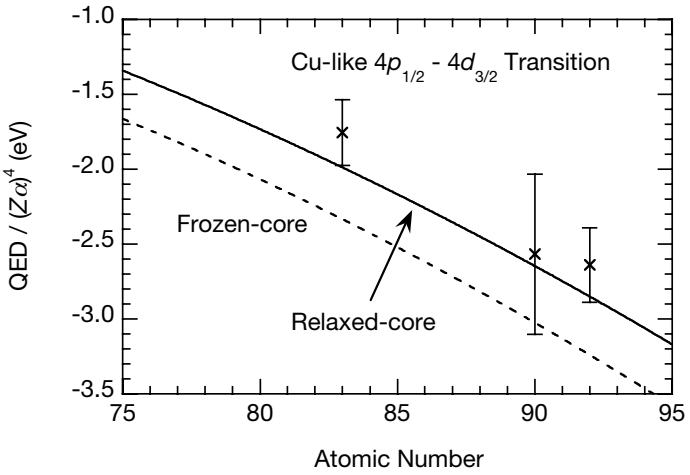

come from rigorous S-matrix calculations, they can be prohibitively difficult to carry out for systems with more than three electrons. In the foreseeable future, RMBPT and RCI will likely remain as the workhorse of high-precision relativistic atomic structure calculations.

Acknowledgments

The work of K.T.C. and M.H.C. was performed under the auspices of the U.S. Department of Energy by the University of California, Lawrence Livermore National Laboratory under Contract No. W-7405-ENG-48. The work of W.R.J. was supported in part by NSF Grant No. PHY-0456828. The work of J.S. was supported in part by NSF Grant No. PHY-0451842.

References

1. I. P. Grant, B. J. McKenzie, P. H. Norrington, D. F. Mayers, and N. C. Pyper, Comput. Phys. Commum. **21**, 207 (1980); B. J. McKenzie, I. P. Grant, and P. H. Norrington, Comput. Phys. Commum. **21**, 233 (1980).
2. J. F. Seely, J. O. Ekberg, C. M. Brown, U. Feldman, W. E. Behring, J. Reader, and M. C. Richardson, Phys. Rev. Lett. **57**, 2924 (1986).
3. P. Mohr, Ann. Phys. **88**, 52 (1974); Phys. Rev. Lett. **34**, 1050 (1975).
4. K. T. Cheng and R. A. Wagner, Phys. Rev. A **36**, 5435 (1987).
5. P. Beiersdorfer, D. Knapp, R. E. Marrs, S. R. Elliot, and M. H. Chen, Phys. Rev. Lett. **71**, 3939 (1993).
6. W. R. Johnson, J. Sapirstein, and K. T. Cheng, Phys. Rev. A **51**, 297 (1995).
7. K. T. Cheng and M. H. Chen, Phys. Rev. A **53**, 2206 (1996).
8. W. R. Johnson, K. T. Cheng and M. H. Chen, "Accurate relativistic calculations including QED contributions for few-electron systems," *in* "Relativistic electronic Structure Theory, Part 2, Applications" P. Schwerdtfeger, *Editor* (Vol. 14, Theoretical and Computational Chemistry, Elsevier, 2004).
9. G. E. Brown and D. G. Ravenhall, Proc. R. Soc. London, Ser. A **208**, 552 (1951).
10. J. Sucher, Phys. Rev. A **22**, 348 (1980).
11. M. H. Mittleman, Phys. Rev. A **4**, 893 (1971); **5**, 2395 (1972); **24**, 1167 (1981).
12. J. Sapirstein, K. T. Cheng, and M. H. Chen, Phys. Rev. A **59**, 259 (2001).
13. S. A. Blundell, P. J. Mohr, W. R. Johnson, and J. Sapirstein, Phys. Rev. A **48**, 2615 (1993).
14. I. Lindgren, H. Persson, S. Salomonson, and L. Labzowski, Phys. Rev. A **51**, 1167 (1995).

©2007 NRC Canada

15. F. Mark and W. H. E. Schwarz, Phys. Rev. Lett., **48**, 673 (1982).
16. R. E. Stanton and S. Havriliak, J. Chem. Phys., **81**, 1910, (1984).
17. Y. K. Kim, F. Parente, J. P. Marques, P. Indelicato, and J. P. Desclaux, Phys. Rev. A **58**, 1885 (1998).
18. W. R. Johnson, S. A. Blundell, and J. Sapirstein, Phys. Rev. A **37**, 307 (1988).
19. A. Chodos, R. L. Jaffe, K. Johnson, C. B. Thorn, and V. W. Weisskopf, Phys. Rev. D **9**, 3471 (1974).
20. J. J. Sakurai, *Advanced Quantum Mechanics* (Addison-Wesley, Reading, MA. 1967).
21. E. R. Davidson, J. Comp. Phys. **17**, 87 (1975).
22. A. Stathopoulos and C. F. Fischer, Comput. Phys. Commun. **79**, 1 (1994).
23. W. R. Johnson and G. Soff, At. Data Nucl. Data Tables, **33**, 405 (1985).
24. J. D. Zumbro, R. A. Naumann, M. V. Hoehn, E. B. Shera, C. E. Bemis, Jr., and Y. Tanaka, Phys. Lett. **167B**, 383 (1986).
25. J. D. Zumbro, E. B. Shera, Y. Tanaka, C. E. Bemis, Jr., R. A. Naumann, M. V. Hoehn, W. Reuter, and R. M. Steffen, Phys. Rev. Lett. **53**, 1888 (1984).
26. J. Sapirstein and K. T. Cheng, Phys. Rev. A **73**, 012503 (2006).
27. J. Sapirstein and K. T. Cheng, Phys. Rev. A **68**, 042111 (2003).
28. S. A. Blundell, Phys. Rev. A **46**, 3762 (1992).
29. K. T. Cheng, M. H. Chen, and J. Sapirstein, Phys. Rev. A **62**, 054501 (2000).
30. M. H. Chen, K. T. Cheng, P. Beiersdorfer, and J. Sapirstein, Phys. Rev. A **68**, 022507 (2003).
31. K. T. Cheng and M. H. Chen, Rad. Phys. Chem., **75**, 1753 (2006).
32. M. H. Chen, K. T. Cheng, W. R. Johnson, and J. Sapirstein, Phys. Rev. A **74**, 042510 (2006).
33. W. R. Johnson, S. A. Blundell, and J. Sapirstein, Phys. Rev. A **37**, 2764 (1988).
34. S. A. Blundell, W. R. Johnson, and J. Sapirstein, Phys. Rev. A **41**, 1698 (1990).
35. M. H. Chen, K. T. Cheng, W. R. Johnson, and J. Sapirstein, Phys. Rev. A **52**, 266 (1995).
36. P. Indelicato and J. P. Desclaux, Phys. Rev. A **42**, 5139 (1990).
37. P. Beiersdorfer, A. L. Osterheld, J. H. Scofield, J. R. Crespo López-Urrutia, and K. Widmann, Phys. Rev. Lett. **80**, 3022 (1998).
38. S. A. Blundell, Phys. Rev. A **47**, 1790 (1993).
39. J. Sapirstein and K. T. Cheng, Phys. Rev. A **64**, 022502 (2001).
40. P. Beiersdorfer, H. Chen, D. B. Thorn, and E. Träbert, Phys. Rev. Lett. **95**, 233003 (2005).
41. G. Plunien and G. Soff, Phys. Rev. A **51**, 1119 (1995).
42. G. Plunien and G. Soff, Phys. Rev. A **53**, 4614 (1996).
43. A. N. Artemyev, V. M. Shabaev, and V. A. Yerokhin, Phys. Rev. A **52**, 1884 (1995)
44. G. S. Adkins and J.Sapirstein, Phys. Rev. A **73**, 032505 (2006); G. S. Adkins, S. Morrison, and J. Sapirstein, unpublished.
45. S. B. Utter, P. Beiersdorfer, E. Träbert and E. J. Clothiaux, Phys. Rev. A **67**, 032502 (2003).
46. E. Träbert, P. Beiersdorfer, and H. Chen, Phys. Rev. A, **70**, 032506 (2004).
47. E. Träbert, P. Beiersdorfer, K. B. Fourier and M. H. Chen, Can. J. Phys., **82**, 1 (2004).
48. W. R. Johnson, S. A. Blundell, and J. Sapirstein, Phys. Rev. A **42**, 1087 (1990).

©2007 NRC Canada